Journal of Theoretical Biology 592 (2024) 111883

Contents lists available at ScienceDirect

Journal of Theoretical Biology

journal homepage: www.elsevier.com/locate/yjtbi

# A model of time-dependent macromolecular and elemental composition of phytoplankton

Anne Willem Omta [a,*], Justin D. Liefer [b], Zoe V. Finkel [c], Andrew J. Irwin [d], Daniel Sher [e], Michael J. Follows [f]

[a] Department of Earth, Environmental, and Planetary Sciences, Case Western Reserve University, 10900 Euclid Avenue, Cleveland, OH 44106, USA
[b] Department of Biology, Mount Allison University, 63B York Street, Sackville, E4L 1A5, New Brunswick, Canada
[c] Department of Oceanography, Dalhousie University, 1355 Oxford Street, Halifax, B3H 4R2, Nova Scotia, Canada
[d] Department of Mathematics and Statistics, Dalhousie University, 6316 Coburg Road, Halifax, B3H 4R2, Nova Scotia, Canada
[e] Leon H. Charney School of Marine Sciences, University of Haifa, Mount Carmel 31905, Haifa, Israel
[f] Department of Earth, Atmospheric and Planetary Sciences, MIT, 77 Massachusetts Avenue, Cambridge, MA 02139, USA

ARTICLE INFO

*Keywords:*
Plankton physiology
Protein
Chl
Dynamics
Stoichiometry

ABSTRACT

Phytoplankton Chl:C:N:P ratios are important from both an ecological and a biogeochemical perspective. We show that these elemental ratios can be represented by a phytoplankton physiological model of low complexity that includes major cellular macromolecular pools. In particular, our model resolves time-dependent intracellular pools of chlorophyll, proteins, nucleic acids, carbohydrates/lipids, and N and P storage. Batch culture data for two diatom and two prasinophyte species are used to constrain parameters that represent specific allocation traits and strategies. A key novelty is the simultaneous estimation of physiological parameters for two phytoplankton groups of such different sizes. The number of free parameters is reduced by assuming (i) allometric scaling for maximum uptake rates, (ii) shared half-saturation constants for synthesis of functional macromolecules, (iii) shared exudation rates of functional macromolecules across the species. The rationale behind this assumption is that across the different species, the same or similar processes, enzymes, and metabolites play a role in key physiological processes. For the turnover numbers of macromolecular synthesis and storage exudation rates, differences between diatoms and prasinophytes need to be taken into account to obtain a good fit. Our model fits suggest that the parameters related to storage dynamics dominate the differences in the C:N:P ratios between the different phytoplankton groups. Since descriptions of storage dynamics are still incomplete and imprecise, predictions of C:N:P ratios by phytoplankton models likely have a large uncertainty.

## 1. Introduction

From culture experiments, it has been well established that phytoplankton chlorophyll-to-carbon (Chl:C) and nitrogen-to-phosphorus (N:P) ratios are highly variable (Droop, 1974; Rhee, 1978; Raven, 1987). These variations are particularly notable under limitation: nutrient-limited phytoplankton store large amounts of C-rich photosynthate-derivates, whereas light-limited phytoplankton can build up N stores in vacuoles (Sterner and Elser, 2002). Several phytoplankton species have been observed to build up large cellular inventories of polyphosphate (Rhee, 1973; Dyhrman, 2016; Solovchenko et al., 2019), which may serve as a storage of both P and energy (Moreno and Martiny, 2018). In addition, phytoplankton groups appear to exhibit systematic variations in their average elemental compositions (Quigg et al., 2003; Sharoni and Halevy, 2020). Such interspecies variations could be due to differences in cell wall structure (Finkel et al., 2016) or a larger storage capacity of large cells compared to smaller cells (Liefer et al., 2018, 2019). It has been observed that elemental ratios of autotrophs impact the growth of herbivores (Sterner and Hessen, 1994; Plath and Boersma, 2001; Boyer et al., 2004). For example, the growth rate of the rotifer *Brachionus rubens* depends strongly on the C:N:P ratio of the ingested algae (Rothhaupt, 1995). Indirectly, even higher trophic levels could be impacted by the elemental ratios of the organisms at the base of the food web (Hessen et al., 2013). Therefore, the theory of Ecological Stoichiometry (Sterner and Elser, 2002; Geider and la Roche, 2002; Klausmeier et al., 2004) suggests that elemental ratios are of central importance to the functioning of ecosystems.

* Corresponding author.
*E-mail address:* anne.omta@case.edu (A.W. Omta).

https://doi.org/10.1016/j.jtbi.2024.111883
Received 13 November 2023; Received in revised form 8 June 2024; Accepted 14 June 2024
Available online 20 June 2024

Spatio-temporal variation in the elemental composition of phytoplankton could also have significant implications for regional and global ocean carbon storage. In particular, C:N and C:P ratios of sinking particulate organic matter determine how much C is exported per amount of N or P (Broecker, 1982; Volk and Hoffert, 1985; Omta et al., 2009). Thus, elemental stoichiometry directly impacts the strength of the biological carbon pump. Recently, a more indirect effect has been suggested: phytoplankton with high C:N ratios would be able to draw down N to lower concentrations than phytoplankton with low C:N ratios (Chien et al., 2023). This would enhance the impact of elemental stoichiometric variations of marine plankton on total carbon storage.

The importance of phytoplankton C:N:P ratios from both ecological and biogeochemical perspectives has stimulated a desire for dynamic, mechanistic models to predict these ratios. Although global ocean simulations most often rely on a fixed elemental composition, some (e.g., Ward and Follows, 2016) have represented flexible stoichiometry following an internal-stores approach (Caperon, 1968; Droop, 1968). Other simulations (Omta et al., 2006, 2007, 2009) have employed the Dynamic Energy Budgets approach (Kooijman, 2000) and similar formulations (Talmy et al., 2014) which separate elemental cell quotas into functional and reserve pools. Allocation-based models typically divide the cellular biomass into several pools with different physiological functions, between which nutrients and energy are allocated according to an optimization principle. For example, Shuter (1979) pioneered a framework that resolved several functional compartments (photosynthetic, biosynthetic, structural and storage) and optimized allocation of carbon to maximize the growth rate. More recently, several modeling studies have explored how such allocation may affect elemental stoichiometry (Flynn, 2001; Pahlow, 2005; Wirtz and Pahlow, 2010; Pahlow and Oschlies, 2013; Toseland et al., 2013; Daines et al., 2014; Nicholson et al., 2018). Furthermore, Ghyoot et al. (2017) formulated a Shuter-type model for the allocation to the autotrophic and heterotrophic machineries in mixotrophs.

To make further progress in the development of credible and useful models for phytoplankton stoichiometry, it is crucial that these models can be tested against observations. A key challenge is that the resolution of phytoplankton data sets tends to be either much higher (at the level of individual enzymes or pathways (Bar-Even et al., 2011; Wu et al., 2015)) or much lower (bulk stoichiometric data (Elrifi and Turpin, 1985; Goldman, 1986)) than the resolution of most plankton physiological models. Such mismatches between modeled and measured variables make constraining the model structure and parameters difficult. In our view, the Ecological Stoichiometry framework offers an appealing approach to close this gap. One of the central ideas underlying this framework is that the elemental composition of the cell is related to the relative abundance of directly measurable key macromolecular pools (as depicted schematically in Fig. 1). These macromolecular pools, in turn, depend upon the physiological state of the organism and the local resource environment. With this framework in mind, we recently formulated models focused on the steady-state allocation of macromolecular pools (Inomura et al., 2020) and cellular storage (Omta et al., 2020).

In aquatic ecosystems, nutrient inputs to the surface tend to be episodic. As a result, phytoplankton populations experience occasional nutrient-replete conditions interspersed with time periods of starvation. To represent the impact of such variability, we have now developed an explicit, dynamic model of functional, macromolecular allocation in algal cells. In this model, the state variables are directly and quantitatively compared to, and constrained by, data from batch-culture experiments (Liefer et al., 2019). The parameters of the model include a set of rate constants governing the flows between those pools. Using a Markov Chain Monte Carlo approach, we identify those model solutions that represent the observations best, confirming that the model structure is appropriate and providing quantitative estimates for the parameter values. Model testing and parameter fitting is first performed in the context of nitrogen uptake and allocation. Carbon and phosphorus flows are then linked and predicted using their known elemental ratios in the different macromolecular pools. We present the model's formulation in Section 2. In Section 3, we present and discuss the models fits to the Liefer et al. (2019) data set for the four algal species. We discuss the prospects for such models and the broader context in Section 4.

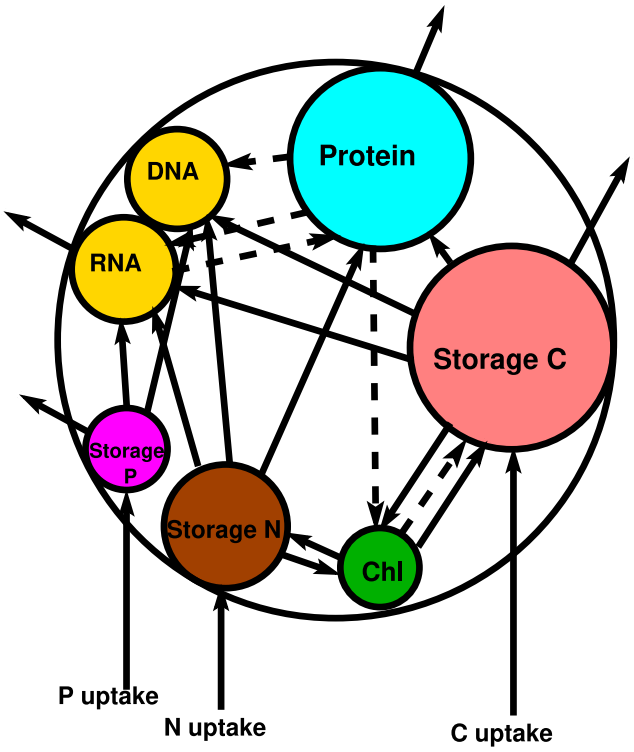


**Fig. 1.** A schematic depiction of the model algal cells with the different compartments; solid lines indicate material fluxes, dashed lines indicate enzymatic action.

## 2. Methods

### 2.1. Model formulation

To represent the physiological basis of variations in algal C:N:P stoichiometry, we resolve several classes of macromolecule (RNA, DNA, protein, carbohydrate, lipids, and Chl) and storage pools of N and P (Fig. 1). Phytoplankton cells store N and P in both organic and inorganic forms in vacuoles, the cytosol (mainly in cyanobacteria), and the chloroplast (Raven, 1987). Together, these intracellular pools typically account for most of the C, N, and P. In the model, each of these pools has its own fixed stoichiometry. The overall fluctuations of intracellular Chl:C:N:P are the result of variations in the resource allocation to the pools.

The uptake of inorganic resources is modeled as a Michaelis–Menten process with size-dependent prior estimates of maximum uptake rates (Litchman et al., 2007). On uptake, inorganic N and P accumulate in storage pools while photosynthate accumulates in a carbohydrate pool. Photosynthesis is formulated and constrained by the measured quantum yield and absorption cross section. Protein, nucleic acids and pigments are synthesized from carbohydrate/lipid and N- and P-storage substrates. We assume that the aggregate of the multiple synthesis reactions leading to the production of the macromolecular components of the cell also exhibits Michaelis–Menten kinetics. This appears reasonable, since there are usually one or a few rate-limiting steps in a series of chemical reactions.

**Table 1**
Description of the parameters with associated units and estimated values. Note that $V$ and $\mu_0$ were not estimated but taken directly from Liefer et al. (2019); the turnover numbers $k_{cat,i}$ were calculated from other parameters using Eq. (16). Error estimates are 1 standard deviation from the posterior parameter distribution.

| Common parameters | | | |
|---|---|---|---|
| Parameter | Description | Units | Value |
| $\langle V_{m,N} \rangle$ | Scaled maximum N uptake rate | fmol/cell $d^{-1}$ $(\mu m^3/cell)^{-0.82}$ | 2.9 ± 0.2 |
| $\langle V_{m,P} \rangle$ | Scaled maximum P uptake rate | fmol/cell $d^{-1}$ $(\mu m^3/cell)^{-0.94}$ | 0.83 ± 0.08 |
| $K_{N\,med}$ | Half-saturation constant for N uptake | μM | 0.1 |
| $\langle K_{pro} \rangle$ | Protein synthesis half-saturation constant | mM (N) | 88 ± 9 |
| $\langle K_{rna} \rangle$ | RNA synthesis half-saturation constant | M (N) | 0.44 ± 0.04 |
| $\langle K_{dna} \rangle$ | DNA synthesis half-saturation constant | mM (N) | 2.6 ± 0.7 |
| $\langle K_{chl} \rangle$ | Chl synthesis half-saturation constant | mM (N) | 125 ± 18 |
| $L_{pro}$ | Protein exudation rate | $d^{-1}$ | 0.0031 ± 0.0013 |
| $L_{rna}$ | RNA exudation rate | $d^{-1}$ | 0.076 ± 0.005 |
| $L_{chl}$ | Chl decay rate | $d^{-1}$ | 0.042 ± 0.006 |
| $R_{C:N,Pro}$ | Protein C:N ratio | – | 3.8 |
| $R_{C:N,DNA}$ | DNA C:N ratio | – | 2.6 |
| $R_{C:N,RNA}$ | RNA C:N ratio | – | 2.6 |
| $R_{C:N,Chl}$ | Chl C:N ratio | – | 13.75 |
| $R_{N:P,DNA}$ | DNA N:P ratio | – | 3.75 |
| $R_{N:P,RNA}$ | RNA N:P ratio | – | 3.75 |

| Individual species parameters | | | | | | |
|---|---|---|---|---|---|---|
| Parameter | Description | Units | *T. pseudonana* | *T. weissflogii* | *O. tauri* | *Micromonas* |
| $V$ | Cell volume | $(\mu m)^3$ | 158 | 1630 | 0.5 | 1.8 |
| $\mu_0$ | Maximum growth rate | $d^{-1}$ | 0.75 | 0.57 | 0.72 | 0.4 |
| $k_{cat,pro}$ | Protein synthesis turnover number | $d^{-1}$ | 11.3 ± 0.2 | 5.7 ± 0.1 | 7.2 ± 0.1 | 6.0 ± 0.1 |
| $k_{cat,rna}$ | RNA synthesis turnover number | $d^{-1}$ | 0.055 ± 0.001 | 0.065 ± 0.001 | 0.080 ± 0.001 | 0.032 ± 0.001 |
| $k_{cat,dna}$ | DNA synthesis turnover number | $d^{-1}$ | 0.050 ± 0.001 | 0.057 ± 0.001 | 0.048 ± 0.001 | 0.0167 ± 0.0002 |
| $k_{cat,chl}$ | Chl synthesis turnover number | $d^{-1}$ | 0.0211 ± 0.0004 | 0.0184 ± 0.0004 | 0.0191 ± 0.0004 | 0.0092 ± 0.0002 |
| $\langle K_C \rangle$ | Scaled C fixation regulatory parameter | fmol(C)/$(\mu m)^3$ | 26 ± 7 | 260 ± 100 | 38 ± 8 | 7.67 ± 0.08 |
| $\langle K_P \rangle$ | Scaled P uptake regulatory parameter | fmol(P)/$(\mu m)^3$ | 0.072 ± 0.006 | 0.070 ± 0.001 | 0.48 ± 0.04 | 0.121 ± 0.009 |

### 2.1.1. Rate equations

Generically, we resolve the cellular quota of each macromolecular pool ($[X_i]$) where $i$ may denote *pr*, protein; *rna*, RNA, *dna*, DNA; *cs*, carbohydrate + lipid ("C storage"); ns, "N storage"; *chl*, Chlorophyll; or *ps*, "P storage". The quota $[X_i]$ are in mol N $cell^{-1}$, except for C storage (mol C $cell^{-1}$) and P storage (mol P $cell^{-1}$). The temporal rates of change (mol $cell^{-1}$ $s^{-1}$) are described as:

$$\frac{d[X_i]}{dt} = \underbrace{S_i}_{\text{synthesis/source}} - \underbrace{\sum_{k\neq i} S_{i,k}}_{\text{consumption}} - \underbrace{L_i[X_i]}_{\text{loss}} - \underbrace{\mu[X_i]}_{\text{division}} \tag{1}$$

with parameters and variables listed in Table 1. The first term on the right $S_i$ represents the rate of synthesis of pool $i$. The second term $\sum_{k\neq i} S_{i,k}$ represents the consumption of pool $i$ in the synthesis of other pools ($k \neq i$); $S_{i,k} = 0$ except if pool $i$ is C, N, or P storage (see schematic in Fig. 1). The third term on the right represents losses at rate $L_i$ (mol $cell^{-1}$ $s^{-1}$), which includes respiration (C storage only), exudation, and degradation of macromolecular machinery, e.g., photodamage to photosystems (Sonoike, 2011; Vass, 2012; Zavafer, 2021). Furthermore, the amount of each compound becomes distributed over a larger number of cells as the organisms divide, i.e., dilution by division (Kooijman, 2000). This is represented by the last term ($\mu[X_i]$), where $\mu$ ($s^{-1}$) is equivalent to the average per capita rate of change of cell density.

The synthesis of protein, RNA, DNA, and chlorophyll is generically represented as a Michaelis–Menten type enzymatic reaction:

$$S_i = k_{cat,i}[X_{icat}] \ \min\left(\frac{[X_{ns}]}{K_i + [X_{ns}]}, \frac{\left(\frac{[X_{cs}]}{R_{C:N,i}}\right)}{K_i + \left(\frac{[X_{cs}]}{R_{C:N,i}}\right)}, \frac{[X_{ps}]R_{N:P,i}}{K_i + [X_{ps}]R_{N:P,i}}\right) \tag{2}$$

In this enzymatic reaction, the *cs*, *ns*, and *ps* storage pools act as substrates for the synthesis of macromolecular pool $i$. Macromolecular pool *icat* acts as the catalyst, with turnover number (maximum net production rate) $k_{cat,i}$ ($s^{-1}$) and half-saturation constant $K_i$ (N mol). For protein synthesis, we assume that RNA is the catalytic pool *icat*. Most of the RNA is in the ribosomes (Bremer and Dennis, 1996) and is thus connected with protein synthesis. Indeed, an increase of the RNA:protein ratio with increasing growth rate is observed across many organisms (Scott et al., 2010). We assume that protein is the catalytic pool *icat* for the synthesis of RNA, DNA, and Chl. $R_{C:N,i}$ and $R_{N:P,i}$ denote the C:N and N:P ratios of the macromolecular pool $X_i$ that is being synthesized. The minimum formulation in Eq. (2) provides for the possibility that stored C, stored N, or stored P is limiting the product formation. The elemental stoichiometry of each macromolecular pool determines which element is limiting the synthesis of that pool. That is, the C:N ratios of DNA and RNA ($C : N_{DNA}$ and $C : N_{RNA}$) are equal to 2.6:1, the C:N ratio of protein ($C : N_{Pro}$) is equal to 3.8:1, and the C:N ratio of Chl is equal to 13.75:1 ($C : N_{Chl}$) (Geider and la Roche, 2002). This means that in some of our simulations, Chl synthesis may be limited by C, while the synthesis of DNA, RNA, and protein is limited by N. Parameter values for $k_{cat,i}$ and $K_i$ are not known a priori as they represent an abstraction of metabolic organization, here constrained by the model-data synthesis.

Although the number of genome copies per cell can vary greatly in prokaryotes (Sukenik et al., 2012), in eukaryotes the genome copy number is normally determined by their reproductive life cycle stage. Indeed, the average DNA content per cell remained approximately constant throughout the experiments (except for *T. pseudonana*, which may have been polyploid (Liefer et al., 2019)). Setting $\frac{d[X_{dna}]}{dt}$ equal to 0 in the quota Eq. (1) for DNA and neglecting any loss or degradation of DNA ($L_{dna} = 0$) leads to the following expression for the population growth rate ($\mu$):

$$\mu = \frac{S_{dna}}{[X_{dna}]} \tag{3}$$

where $S_{dna}$ is calculated from Eq. (2). This expression is then used to solve the quota Eqs. (1) for the other pools.

### 2.1.2. Storage pools

Although (membrane) lipids are part of the cell structure, they are not part of the synthetic machinery. Therefore, we use a single

"storage C" pool to represent both carbohydrates and lipids. We have the following dynamic equation for this pool:

$$\frac{d[X_{cs}]}{dt} = S_{cl,C} - S_C - r_C + \sum_i R_{C:N,i}[X_i]L_i - \mu[X_{cs}] \tag{4}$$

with $S_{cl,C}$ the gross photosynthesis rate, $S_C$ the C used for biosynthesis and $r_C$ the respiration costs.

The gross photosynthesis rate, $S_{cl,C}$, (moles C cell$^{-1}$ s$^{-1}$) is evaluated from the measured photo-physiological parameters of the simulated laboratory cultures (Liefer et al., 2018) in the following way:

$$S_{cl,C} = [X_{chl}]\frac{IYa^*}{8}\left(1 - \frac{[X_{cs}]}{K_C}\right) \tag{5}$$

where $I$ is the imposed light intensity, $Y$ the measured quantum yield of Photosystem II (PS II) photochemistry, and $a^*$ the measured spectrally averaged Chl a-specific light absorption cross-section. The division by 8 is because 4 electrons need to be fed into the Calvin cycle per C atom fixed (Bolton and Hall, 1991) and 2 photons need to be absorbed (one by PS II and one by PS I) per excited electron (Falkowski and Raven, 2007). The prasinophytes appear to down-regulate net C fixation as the intracellular amount of C storage increases. In the context of internal stores models (Caperon, 1968; Droop, 1968; Caperon and Meyer, 1972; Legovic and Cruzado, 1997; Klausmeier et al., 2004), this could be represented implicitly by a minimum N:C or maximum C:N quota. However, this raises the question of what determines such a minimum or maximum quota. A possible answer is that the net uptake of non-limiting nutrients is inhibited when the storage takes up a too large of a fraction of the cell volume. To describe this for both C and P, we use a linearized version of the Rhee (1973) formulation that has been applied previously to describe the regulation of nutrient uptake in phytoplankton (Bougaran et al., 2010; Omta et al., 2020). Since Rhee (1973) originally used this formulation for P uptake inhibition, it is not a priori obvious that it can be used for C as well. Even so, we think that our formulation is applicable to C for the following reasons:

1. The problem of storing excess quota in a small cell is essentially the same for C and P (although probably more severe for C), since both elements form polymers that accumulate in cellular compartments that take up intracellular space (Sicko-Goad et al., 1984; Chiovitti et al., 2004).
2. If a different formulation than Rhee (1973) would be more appropriate for C, then linearization would still lead to the formulation that we used.

The actual physiological mechanism behind this inhibition of net C accumulation is uncertain, because it is very difficult to distinguish between C exudation, respiration, and various photoprotective mechanisms. The linearized inhibition term $\left(1 - \frac{[X_{cs}]}{K_C}\right)$ in Eq. (5) can be interpreted as describing any of these processes or a combination of them.

The C used for biosynthesis ($S_C$) equals:

$$\begin{aligned} S_C \equiv & R_{C:N,pro}S_{pro} + R_{C:N,rna}S_{rna} \\ & + R_{C:N,dna}S_{dna} + R_{C:N,chl}S_{chl} \end{aligned} \tag{6}$$

The total respiration ($r_C$) consists of two terms, one related to maintenance and one related to biosynthesis:

$$r_C = \underbrace{r_0[X_{cf}]}_{\text{Maintenance}} \underbrace{+r_1 S_N}_{\text{Biosynthesis}} \tag{7}$$

$[X_{cf}]$ is the amount of C in functional macromolecules (in pmol C/cell):

$$[X_{cf}] \equiv \sum_i R_{C:N,i}[X_i]$$

We take $r_0$ equal to 0.1 d$^{-1}$, representing the average maintenance respiration of various algal species (Geider and Osborne, 1989), and $r_1$ equal to 2 mol C per N-mol functional biomass, which corresponds to the total energetic costs of the conversion of nitrate into protein (Omta et al., 2020). As these parameters are kept at constant values, they are excluded from the parameter estimation.

Inorganic N and P from the medium are taken up into the N and P storage pools. We assume that the nutrient uptake rate is not limited by the size of the cellular protein pool, because phytoplankton cells typically allocate only a small fraction of their proteome toward nutrient transport (Thangaraj et al., 2021; Zimmerman et al., 2023). Prior distributions for the maximum uptake rate are based on empirical and theoretical allometric constraints (Litchman et al., 2007). We model the uptake of dissolved inorganic nitrogen (DIN) from the medium ($N_{med}$ in μM) as following Michaelis–Menten kinetics:

$$\frac{dN_{med}}{dt} = -V_{m,N}X\frac{N_{med}}{K_{Nmed} + N_{med}} \tag{8}$$

with $X$ the cell density. The maximum N uptake rate ($V_{m,N}$) is estimated by fitting the model to the data (see Appendix A below for details). We were unable to estimate the half-saturation constant of N uptake ($K_{Nmed}$) or the N uptake affinity ($\frac{V_{m,N}}{K_{Nmed}}$) directly from the data, because that would require very precise measurements of the uptake rate as a function of the DIN concentration at the transition point from the exponential to the stationary growth stage. We use a value of 0.1 μM for $K_{Nmed}$ for all species, approximately the average across phytoplankton of various sizes and measured under various DIN concentrations (Smith et al., 2014). Models of batch cultures are rather insensitive to the precise value of whichever parameter other than the maximum uptake rate is used to describe the uptake curve, be it the half-saturation constant or the uptake affinity. As a result, any temperature- or size-dependence of either one of these parameters has essentially no impact on the fits. Therefore, we do not account for observed variations in the half-saturation constant (or the uptake affinity) as a function of size and ambient DIN concentration (Smith et al., 2014).

The N for synthesizing the macromolecules is taken out of the N storage pool; N from decayed chlorophyll is returned to the storage. Conservation of mass then leads to:

$$\frac{d[X_{ns}]}{dt} = V_{m,N}\frac{N_{med}}{K_{Nmed} + N_{med}} - S_N + [X_{chl}]L_{chl} - \mu[X_{ns}] \tag{9}$$

with $S_N$ the N used for biosynthesis:

$$S_N \equiv S_{pro} + S_{rna} + S_{dna} + S_{chl} \tag{10}$$

The dynamics of the P storage ($[X_{ps}]$ in mol P/cell) is driven by uptake, usage for the synthesis of functional macromolecules, and dilution by division. P uptake is assumed to be saturated with regard to the phosphate in the medium, since the organisms in these batch cultures are N-limited. The P uptake rate is regulated by the internal storage in a manner analogous to C uptake. This leads to the following dynamic equation:

$$\frac{d[X_{ps}]}{dt} = \underbrace{V_{m,P}\left(1 - \frac{[X_{ps}]}{K_P}\right)}_{\text{Uptake}} \underbrace{-S_P}_{\text{Biosynthesis}} \underbrace{-\mu[X_{ps}]}_{\text{Dilution by division}} \tag{11}$$

with $S_P$ the P used for biosynthesis:

$$S_P \equiv R_{P:N,rna}S_{rna} + R_{P:N,dna}S_{dna} \tag{12}$$

### 2.2. Parameter estimation

The data that we use to estimate the model parameters are a set of batch culture experiments (Liefer et al., 2019). During the first stage of the experiments, the cultures were kept in steady-state N-replete growth under a subsaturating irradiance (85 μE m$^{-2}$ s$^{-1}$, 12 h light per day) and a near-optimum temperature, which was 18 °C for all species except *Micromonas* for which the growth temperature was 6 °C. After sampling at steady-state exponential growth, the cultures were diluted with N-free media to induce N starvation. After this dilution, DIN concentrations were between 12 and 35 μM. The cultures kept growing

exponentially for a few days before reaching stationary phase. DIN in the medium, cell density, and cellular pools of total N, protein, RNA, DNA, Chl, and storage C (carbohydrates and lipids) were all measured. We calculate the storage N as the difference between the total cellular N and the N in protein, RNA, DNA, and Chl. Thus, storage N includes both inorganic storage and organic N-containing molecules, including amino acids. Storage P has been calculated as the difference between the total cellular P and the P in RNA, DNA, and phospholipids (Liefer et al., 2019). Simultaneous analysis of the C:N:P stoichiometry allowed for a dynamically constrained complete quantification of nutrient budgets, including un-assayed components.

Parameters estimated are the biosynthetic rate coefficients for the material flows depicted by arrows in Fig. 1. The half-saturation constants $K_i$ (in mol/cell) are assumed to scale linearly with the cell volume $V$:

$$K_i = \langle K_i \rangle V \tag{13}$$

The maximum N and P uptake rates ($V_{m,N}$, $V_{m,P}$) are assumed to scale allometrically in accordance with empirical observations (Edwards et al., 2012):

$$V_{m,N} = \langle V_{m,N} \rangle V^{0.82} \tag{14}$$

$$V_{m,P} = \langle V_{m,P} \rangle V^{0.94} \tag{15}$$

We limit the number of free model parameters by assuming that the rescaled parameters ($\langle K_i \rangle$, $\langle V_{m,N} \rangle$, $\langle V_{m,P} \rangle$) are constant and have the same values for all organisms. The rationale behind this assumption is that the same or similar processes, enzymes, and metabolites play a role in nutrient uptake and macromolecular synthesis across the different species.

We use a Metropolis algorithm, as described by Omta et al. (2017, 2020), for the parameter estimation (further details on both the data and the algorithm are given in Appendix A). The initial values of the model state variables (e.g., cell density, macromolecular quotas, nitrate concentration) are drawn from a normal distribution around the mean measured values with a standard deviation equal to the reported measurement error. The model is integrated numerically forward in time, leading to predictions of the time-dependent values of the state variables. A least-squares evaluation of the model-data difference is performed, the parameter values modified and the integration repeated. In subsequent integrations, parameters that either improve upon or slightly degrade the goodness-of-fit, relative to the prior simulation, are saved while others are discarded. Eventually, the parameter distributions stabilize. We visualize the skill of the simulations with these stable parameter distributions using Taylor diagrams (Taylor, 2001).

## 3. Results and discussion

The Liefer et al. (2019) batch culture data cover the transition from exponential growth to starvation for two diatom (*T. pseudonana* and *T. weissflogii*) and two prasinophyte species (*O. tauri* and *Micromonas*). After depletion of the DIN, the populations continue to grow for up to two days. Subsequently, the populations enter the true starvation stage, during which the cell numbers are either stable or show a modest decline. The cellular contents of Chl, protein, and RNA decrease for most species during this stage, whereas cellular DNA was observed to remain approximately stable (Liefer et al., 2019). This was one of the reasons behind our model assumption that $\frac{d[X_{dna}]}{dt} = 0$, which led to Eq. (3) for the population growth. Furthermore, the diatoms show a marked increase in the amount of storage C (carbohydrates and lipids) per cell over the course of the experiments. As explained in Section 2.1, the biosynthesis rates are determined by the internal C, N, and P quota (Eq. (2)). Furthermore, the model includes uptake regulation of C and P (Eqs. (4) and (11)). We were unable to parameterize uptake regulation of the limiting nutrient N, since storage N was too low in the experiments. Rather, we use the flow of N to constrain the key biosynthesis parameters.

In Section 3.1, we perform a parameter estimation to test whether this model structure is compatible with the Liefer et al. (2019) data. By exploiting the known stoichiometry of the macromolecular pools we can link simulations of non-limiting C and P (Section 3.2), which requires additional consideration of storage pools and highlights some key taxonomic differences between the four species.

### 3.1. Simulations and parameter estimation

Since N was the limiting nutrient in the Liefer et al. (2019) experiments, we assume that biosynthesis rates were ultimately driven by the amount of available N. Therefore, most of the parameters (i.e., $\langle V_{m,N} \rangle$, $\langle K_i \rangle$, and $L_i$) are estimated from fits of the flow of N through the system. To limit the number of free parameters in the model, we assume that the loss rates of macromolecules ($L_i$) are the same for all the different species. We obtain reasonably good fits for the macromolecular pools using this assumption (see Fig. 3 and Supplementary Material), even though there does appear to be some interspecies variation in the macromolecular loss rates (in particular for Chl). The temporal changes in the C and P contents of the macromolecular pools constrain $\langle V_{m,P} \rangle$, $K_C$, and $K_P$.

To estimate the turnover numbers $k_{cat,i}$ for the synthesis of protein, DNA, RNA, and Chl, we assume that these macromolecular pools are synthesized at maximum rates during the N-replete stage. Thus, Eq. (2) simplifies to $S_i = k_{cat,i}[X_{icat}]$, with macromolecular pool $icat$ acting as the catalyst for the synthesis of pool $i$. Furthermore, we assume that $\frac{d[X_i]}{dt} = 0$ and we use that $S_{i,k} = 0$ if pool $i$ is protein, DNA, RNA, or Chl. From Eq. (1), we then obtain for the turnover numbers:

$$k_{cat,i} = \frac{(\mu_0 + L_i)\,[X_i]}{[X_{icat}]} \tag{16}$$

with $\mu_0$ the maximum growth rate measured during the N-replete stage. The turnover numbers $k_{cat,i}$ are calculated from Eq. (16), using for $[X_i]$ and $[X_{icat}]$ the cellular quotas of pools $i$ and $icat$ at the beginning of the N-starved (post-dilution) stage. If pool $i$ is protein, then pool $icat$ is RNA; pool $icat$ is protein if pool $i$ is DNA, RNA, or Chl (see Section 2.1.1). We neglect any changes in the turnover numbers between different growth stages, since we are unable to estimate such changes based on the available data. Furthermore, major changes in the turnover numbers appear unlikely, since the temperature was kept constant throughout each experiment.

Posterior means and standard deviations of the parameters are listed in Table 1. As an example of the model fits, we show the fitted cell density and concentrations of protein, RNA, storage N, Chl, and DIN in the medium for *T. pseudonana* (Fig. 2). For the other species, these fitted nitrogen pools are shown in the online Supplementary Material. As can be seen in Fig. 2a–d, the growth of the *T. pseudonana* population and the dynamics of its cellular protein, RNA, and storage N are represented well by the model. Most of the misfit between modeled and measured Chl (Fig. 2e) can be explained by *T. pseudonana* having a relatively high net Chl decay rate compared to the other species. Such interspecies differences are not resolved, as we assumed the macromolecular decay rates to be the same for all species. Modeled DIN decreases faster than observed (Fig. 2f), which likely reflects interspecies variation in N uptake not captured by the allometric scaling. For a quantitative assessment of the goodness-of-fit for each of the 4 species, Taylor diagrams of the cell density and concentrations of protein, RNA, Chl, and DIN in the medium are shown in Fig. 3. In general, the Taylor diagrams indicate good fits of the model to the data, in terms of the timing and amplitudes of the respective state variables. The synthesis turnover numbers tend to be lower for *Micromonas* than for the other species, probably because *Micromonas* was grown at a lower temperature (6 °C) than the other phytoplankton species (18 °C). For the prasinophytes, protein and RNA show less variation in the model than in the data. This is probably due to systematic differences between the prasinophytes and diatoms not captured by the allometric scaling.

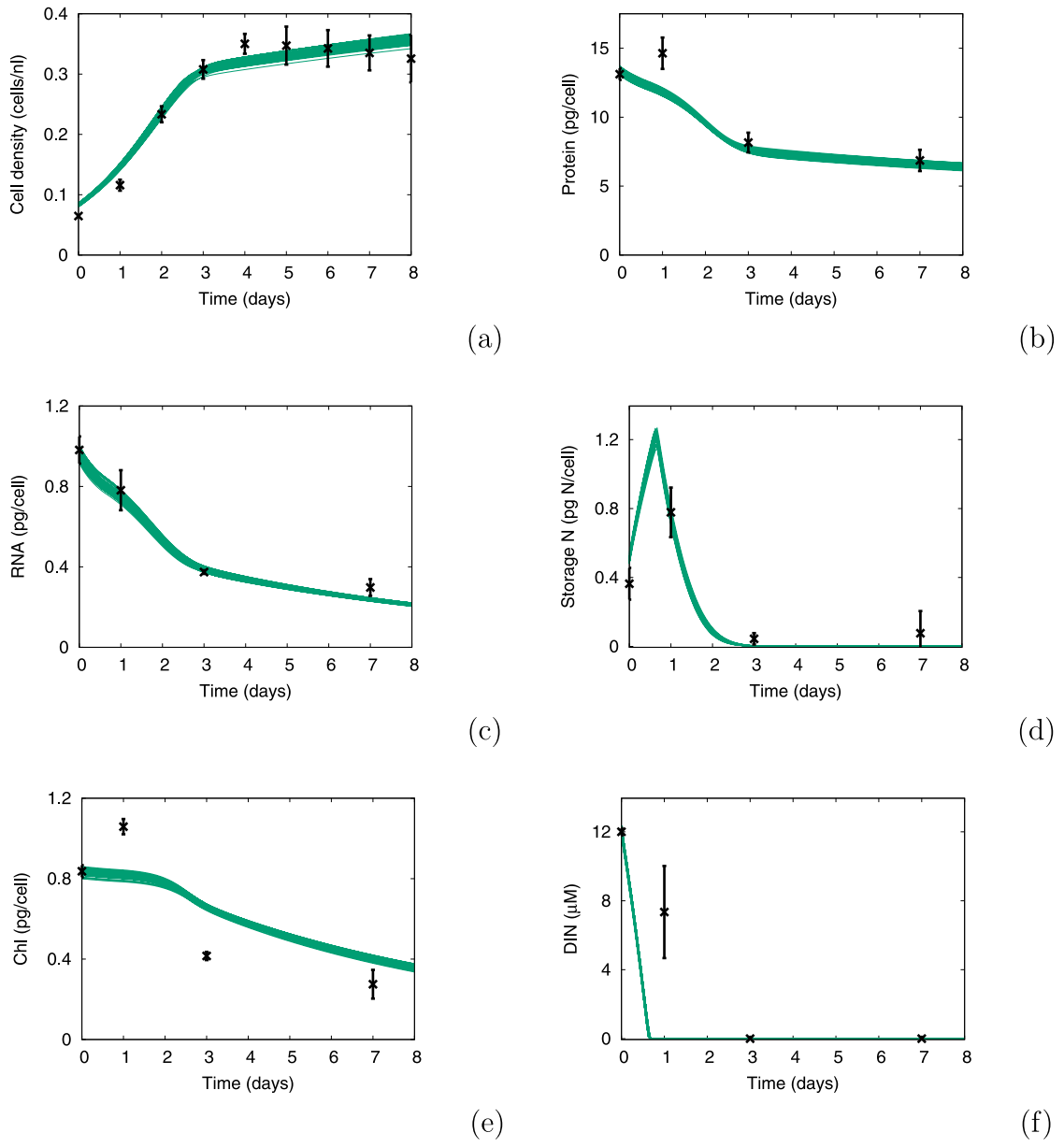


**Fig. 2.** Fits for *T. pseudonana*: (a) cell density, (b) protein concentration, (c) RNA concentration, (d) N storage concentration, (e) chlorophyll concentration, (f) DIN concentration in the medium.

The fitted net decay in cellular Chl likely reflects the difference between Chl turnover and regeneration. If Chl regeneration were negligible, then one would expect the estimated net decay rate to be approximately equal to measured Chl turnover rates. Instead, the estimated net decay rate of Chl is significantly lower than measured Chl turnover rates (2–8 $d^{-1}$) (Riper et al., 1979), which is consistent with continued Chl regeneration even during the starvation stage. Possibly, the organisms are maintaining their Chl to be able to recover quickly once the N starvation is relieved. It has been suggested that such a strategy is used by various plankton species (Halsey and Jones, 2015). There is more Chl decay in the diatoms than in the prasinophytes. This appears to be related to differences in the physiological responses of these two groups of phytoplankton to the severe N starvation. While the diatoms alter their composition, the prasinophytes have a more static composition. In particular, the large amounts of stored C accumulated by the diatoms (see Section 3.2) likely allow them to start growing again as soon as N starvation is relieved. In contrast, the prasinophytes do not have the intracellular space to accumulate much stored C. For these organisms, it is probably important to maintain as much of their photosynthetic capacity as possible for recovery after N resupply. This is consistent with measurements that indicated that diatoms decrease their Chl-a during N starvation, whereas prasinophytes rely more on mechanisms such as non-photochemical quenching to dissipate excess absorbed light energy (Liefer et al., 2018).

### 3.2. Interspecies differences in storage accumulation

Any cell has a limited internal volume, some of which needs to be allocated to organelles. Diatoms appear to have significant "surplus" volume available for storage due to their relatively large size. Furthermore, diatoms have a lower size scaling exponent than most other taxa (Finkel et al., 2016). Indeed, it is well established that diatoms are able to accumulate large storages of C, N, and P (Caperon and Meyer, 1972; Conover, 1975; Lomas and Glibert, 2000; Díaz et al., 2008; Moreno and Martiny, 2018; Jensen et al., 2020). Not much is known about storage accumulation in prasinophytes, but it appears plausible that these organisms simply do not have much

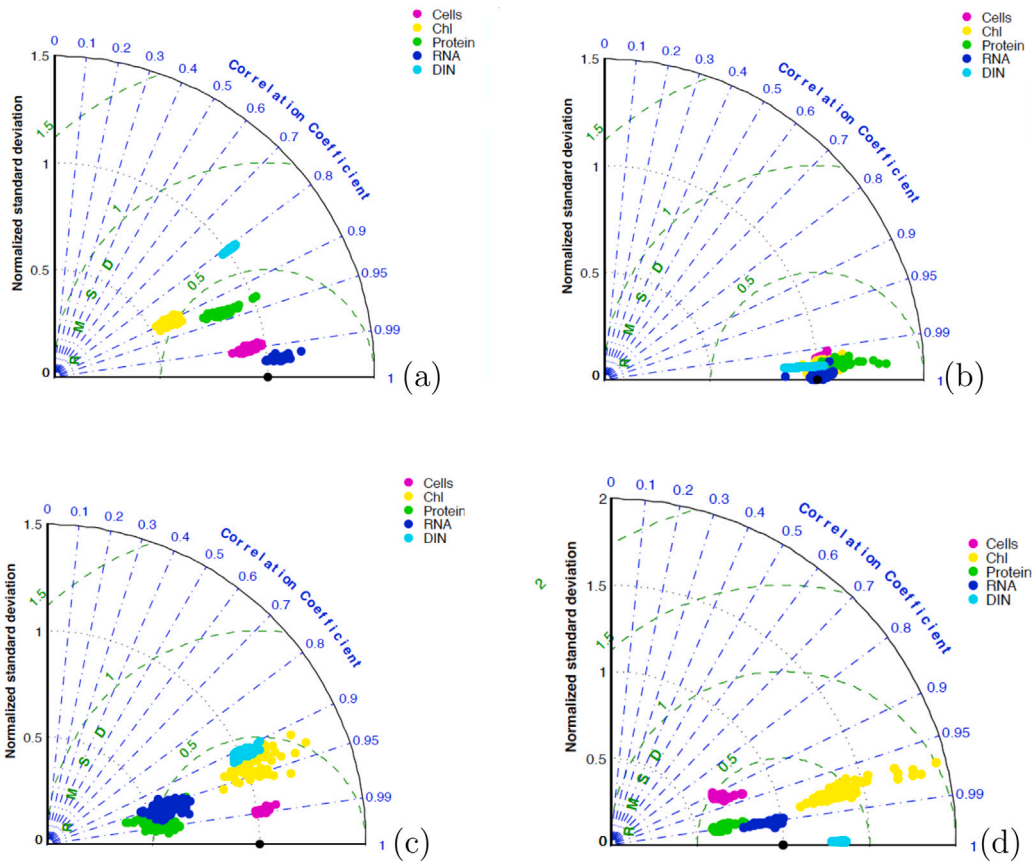


**Fig. 3.** Taylor diagrams for fits of the model to measurements on *T. pseudonana* (a), *T. weissflogii* (b), *O. tauri* (c), *Micromonas* (d). In contrast with conventional Taylor diagrams, different data (i.e., macromolecular pools for each species) are compared with simulations within each diagram. To compare fits to data with different standard deviations within the same diagram, the standard deviation of the data is normalized to 1. The distance between the simulations (colored points) and the data (black) indicates the normalized centered-pattern root-mean-square distance, whereas the cosine of the azimuthal angle corresponds with the correlation coefficient ($r$).

volume left over for nutrient storage. For example, any C storage in prasinophytes appears to be highly localized in the form of microscopic starch granules (Ral et al., 2004; Deschamps et al., 2008). In the Liefer et al. (2019) experiments, the diatoms had significant amounts of storage N during the exponential growth stage, while the prasinophytes appeared to have none (see Supplementary Material). The structure of our model, in which "storage N" is used as a substrate for the synthesis of functional macromolecules, therefore appears more appropriate for the diatoms than for the prasinophytes. Even so, small phytoplankton may build up N reserve in the form of polypeptides, amino acids, or proteins (Raven, 1987). Indeed, prasinophyte population growth continued even after depletion of DIN in the medium, which suggests that these organisms utilized some form of intracellular N. Several types of phytoplankton have been shown to reallocate photosynthetic protein during N starvation (Tolonen et al., 2006; Hockin et al., 2012; Simionato et al., 2013). Some such reallocation probably takes place even within the prasinophytes, although these organisms appear to be maintaining most of their photosynthetic capacity under N starvation. Alternatively, the organisms may have been utilizing dissolved organic compounds that they had exuded earlier. A similar phenomenon has been observed in *E. coli*, which exudes and then consumes acetate during diauxic growth (Sundya et al., 2012; Enjalbert et al., 2013, 2015). Indeed, several algal species are known to utilize dissolved organic nitrogen (Berman et al., 1991; Palenik and Morel, 1991; Pantoja and Lee, 1994; Sipler and Bronk, 2015; Li et al., 2016). Finally, we note that population growth typically continued for only one or two days after DIN had been exhausted and that the growth rates were low ($<0.2\ d^{-1}$).

Although biosynthesis rates are generally not determined by the non-limiting nutrients C and P, describing their dynamics is important for predicting the C:N:P ratios. During the N-starvation phase, the diatoms accumulated significantly larger amounts of "stored" C (carbohydrates and lipids) than did the prasinophytes. This difference is illustrated in the left-hand panels of Fig. 4. We use the measured photophysiological parameters (the absorption cross-section $a^*$ and the quantum yield of PSII $Y$) (Liefer et al., 2018) and the biosynthesis parameters estimated in Section 3.1 to predict the accumulation of newly fixed carbon (purple curves in Fig. 4). These predictions match the observed accumulation of stored C in *T. pseudonana* (Fig. 4a) within a factor of two, and in *T. weissflogii* (Fig. 4c) within 20%. This is consistent with the interpretation that the diatoms used most of the linear electron flow to build up intracellular C storage. For the prasinophytes, the interpretation of the electron flow in terms of C storage (purple curves) leads to a significant overestimate of the C accumulation (Fig. 4e/g), indicating that a large fraction of the electron flow from PSII was diverted elsewhere. The inclusion of inhibition of net C fixation at high cellular C quota (described by Eq. (5)) leads to the green curves in Fig. 4, which are fitted through optimization of the regulatory parameter $K_C$. We estimate the value of this parameter for each species individually. The purple and green curves mostly overlap for the diatoms, which suggests that they used most of the absorbed light to build up large amounts of carbohydrate and lipid (either inside the cell or at the cell surface). The purple and green curves are very different for the prasinophytes, which suggests that they either used much of the absorbed light in pathways other than C fixation or respired/exuded much of their fixed C. Direct measurements of the accumulation of dissolved organic C would be a means to determine the importance of the exudation pathway.

All four phytoplankton species in the Liefer et al. (2019) experiments had significant amounts of P storage. To constrain the flow of P, we estimate $\langle V_{m,P} \rangle$ (a common value across species with allometric

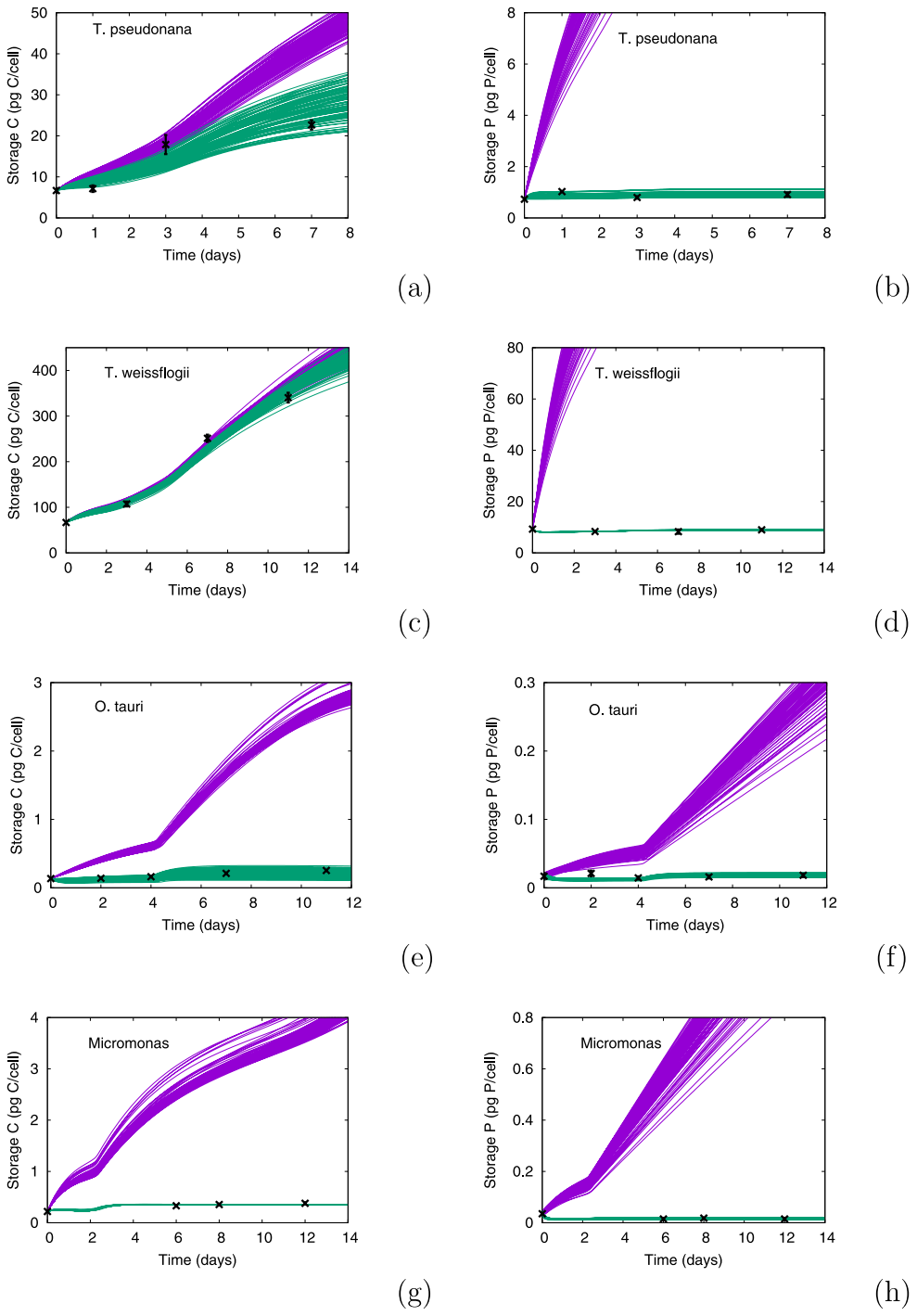


**Fig. 4.** No C uptake regulation needs to be included in the model to reproduce the C accumulation in the diatoms, whereas C uptake regulation needs to be included to reproduce the C accumulation in the prasinophytes. For all species, regulation of P uptake needs to be included. Purple curves indicate simulations without uptake regulation, whereas green curves indicate fits with uptake regulation. The different curves are 80 randomly drawn simulations with parameter sets accepted by the Metropolis algorithm. The widths of the composite curves reflect the uncertainties in the fits, according to the algorithm. Left panels: simulated C storage for *T. pseudonana* (a), *T. weissflogii* (c), *O. tauri* (e), *Micromonas* (g); right panels: simulated P storage for *T. pseudonana* (b), *T. weissflogii* (d), *O. tauri* (f), *Micromonas* (h).

scaling) and $K_P$ (estimated for each species individually). Fits of the storage P to Eq. (11) are shown in Fig. 4. In contrast with storage C, storage P does not appear to increase significantly during the stationary stage in most of the species. The linearized uptake inhibition formulation (Eq. (11)) appears to describe the dynamics of the P storage reasonably well. Nevertheless, there exist high correlations between estimates of $\langle V_{m,P} \rangle$ and $K_P$: $r^2 = 0.59$, $r^2 = 1.00$, $r^2 = 0.57$, $r^2 = 0.45$, for *T. pseudonana*, *T. weissflogii*, *O. tauri*, and *Micromonas*, respectively. Due to these correlations, a rather narrow prior distribution needed to be imposed on $\langle V_{m,P} \rangle$ to constrain $K_P$ (see Appendix A). Although there is reasonably good overall agreement between the model and the data with regard to the overall C:N and C:P ratios for all 4 species (see simulations in Fig. 5), the modeled C:N ratios show larger increases than observed in the diatoms and smaller increases than observed in O. tauri. Again, this probably reflects variations in N and P uptake rates that are not captured by the allometric scaling. In general, there exists a trade-off between minimizing the number of degrees of freedom (e.g., by assuming allometric scaling) and optimizing the goodness-of-fit.

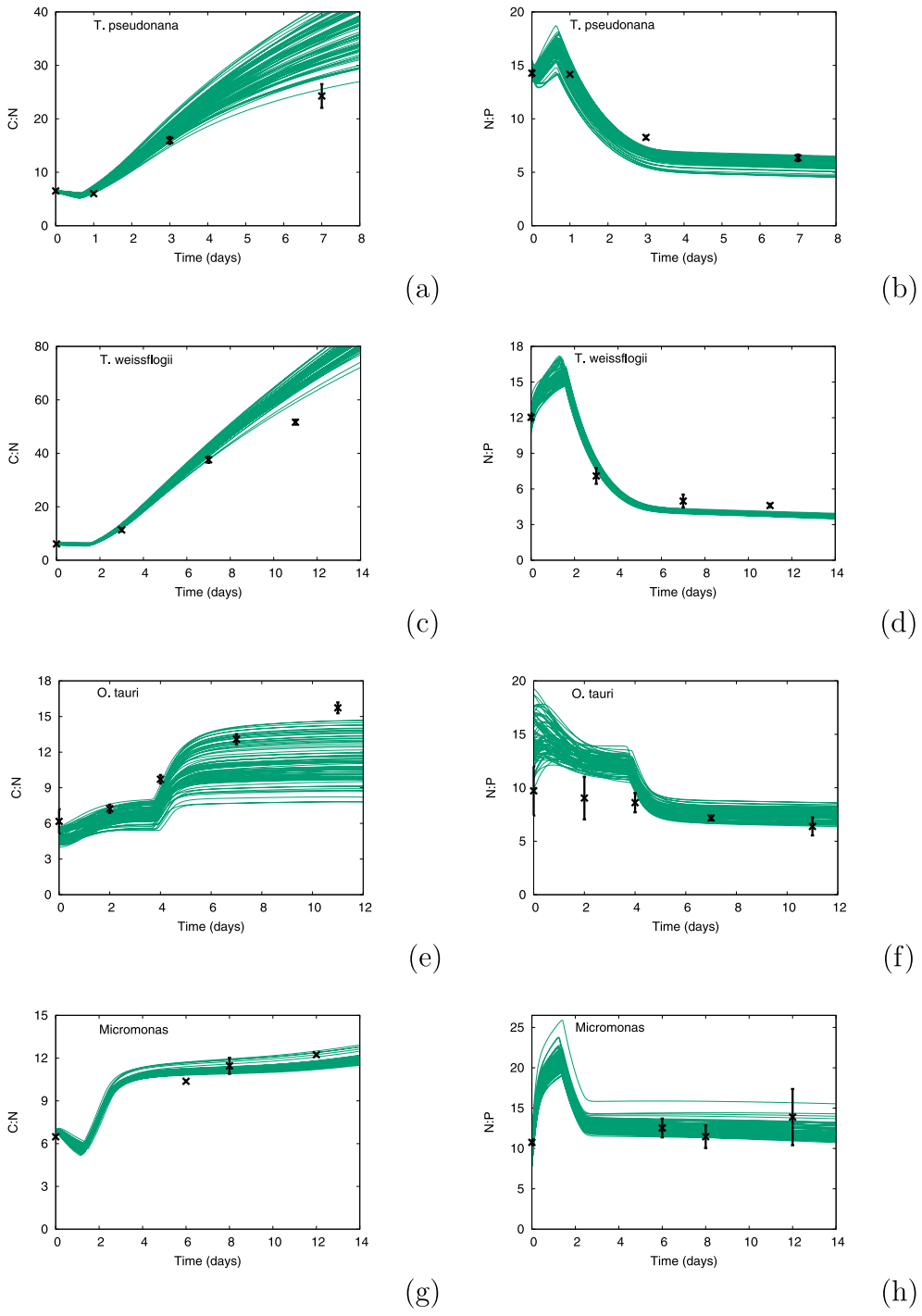


**Fig. 5.** Left panels: simulated C:N ratios for *T. pseudonana* (a), *T. weissflogii* (c), *O. tauri* (e), *Micromonas* (g); right panels: simulated N:P ratios for *T. pseudonana* (b), *T. weissflogii* (d), *O. tauri* (f), *Micromonas* (h). All the simulations correspond to the green curves in Fig. 4 including uptake regulation.

## 4. Conclusion

We have constructed a phytoplankton physiological model that includes several macromolecular pools with the aim of representing phytoplankton Chl:C:N:P ratios. Using this model and batch culture data from Liefer et al. (2019), we have estimated biosynthesis parameters for two diatom and two prasinophyte species. We found that the data on the four different species can be fitted using a single set of allometrically scaled maximum nutrient uptake rates and half-saturation constants (i.e., a subset of key parameters). In our view, this facilitates implementation of the model in ocean ecosystem models, since parameter values that are unknown for certain species or functional groups can be inferred from allometric scaling relationships.

The largest differences between the diatoms and prasinophytes are related to storage, which is not captured by the allometric scaling. This is particularly clear under starvation, even though both phytoplankton groups need to divert excess photosynthetic energy to protect against photodamage. However, these two groups appear to use different strategies toward this aim. In particular, the parameter estimation indicates that in the experiments, the diatoms used most of the electrons leaving PSII to build up large C stores. In contrast, the

prasinophytes must have exuded much C or diverted electrons into alternative pathways. Indeed, a previous set of experiments indicated that prasinophytes direct light energy toward photoprotective pathways. Direct measurements of the accumulation of dissolved organic C would be a means to determine whether the exudation is important as well.

In our view, there is a potentially important corollary to our results. If the allocation to different functional pools is similar across phytoplankton groups but the amount of storage varies strongly, then variations in the storage probably dominate interspecies variations in stoichiometry. So far, internal stores models have mostly focused on the relationship between the *limiting* nutrient quota and the growth rate of the organisms. By contrast, the largest interspecies differences in C:N:P stoichiometry in the experiments considered here are due to the accumulation of the *non-limiting* C and P. Since descriptions of the dynamics of non-limiting nutrient stores ('luxury uptake') are still incomplete and imprecise, predictions of C:N:P ratios by phytoplankton models likely have a large uncertainty. To represent non-limiting nutrient stores accurately in models, dedicated experiments may be helpful. These could focus on the relationships between growth rate, external nutrient concentration, and light intensity on one hand and the accumulation of luxury stores on the other hand.

## Funding

This work was supported by the Simons Collaboration on Computational Biogeochemical Modeling of Marine Ecosystems/CBIOMES (Grant ID: 549931, MJF). Furthermore, the authors are grateful for support from the Gordon & Betty Moore Foundation (Grant number GBMF #3778), the Natural Sciences and Engineering Research Council of Canada, Canada to AJI and ZVF, and the United States-Israel Binational Science Foundation, Israel (Grant number 2010183 to DS and MJF).

## CRediT authorship contribution statement

**Anne Willem Omta:** Conceptualization, Formal analysis, Investigation, Visualization, Writing – original draft, Writing – review & editing, Software. **Justin D. Liefer:** Conceptualization, Writing – review & editing. **Zoe V. Finkel:** Conceptualization, Funding acquisition, Writing – review & editing. **Andrew J. Irwin:** Conceptualization, Funding acquisition, Writing – review & editing. **Daniel Sher:** Conceptualization, Writing – review & editing. **Michael J. Follows:** Conceptualization, Funding acquisition, Project administration, Supervision, Writing – original draft, Writing – review & editing.

## Declaration of competing interest

The authors declare that they have no known competing financial interests or personal relationships that could have appeared to influence the work reported in this paper.

## Acknowledgments

The authors would like to thank Chris Follett for helpful discussions.

## Appendix A. Parameter estimation procedure

We use a Metropolis–Hastings algorithm (Metropolis et al., 1953; Hastings, 1970) to fit our model to the N-starved measurements. One key feature of Bayesian methods, such as the Metropolis–Hastings algorithm, is the possibility to include a priori knowledge about the system in the *prior* distributions of the parameters. The parameter estimation procedure then uses both the prior parameter distributions and the data to provide *posterior* parameter distributions: an update of our knowledge about the system (Lambert, 2018). Here we use broad ('uninformative') prior distributions to avoid subjective choices as much as possible. For most parameters, the only requirement is that they must have positive values. One exception is the pair $\langle V_{m,P} \rangle$ (scaled maximum P uptake) and $K_P$ (P uptake inhibition parameter) due to their strong correlation (see Section 3.2). Without a prior on either $\langle V_{m,P} \rangle$ or $K_P$, neither parameter can be constrained. The prior distribution for $\langle V_{m,P} \rangle$ is based on laboratory measurements of phosphate uptake *by T. pseudonana* and *T. weissflogii* (Terry, 1982; Parslow et al., 1984). Since $\langle V_{m,P} \rangle$ cannot be negative, we assume log-normally distributed priors (median 0.7 fmol P/cell $d^{-1}$ $(\mu m^3/cell)^{-0.94}$, standard deviation 0.14 fmol P/cell $d^{-1}$ $(\mu m^3/cell)^{-0.94}$). For $\langle V_{m,N} \rangle$ (scaled maximum N uptake), we require that it must be sufficiently high to allow for the observed intracellular N accumulation during the N-replete stage. This means that $V_{m,N} \geq \mu_0[X_{t,0}]$ (with $[X_{t,0}]$ the total N per cell at the beginning of the N-starved stage).

The algorithm requires the data distribution as input to calculate the likelihood ratio (Omta et al., 2017). The data under consideration are likely not normally distributed, because the error bars reflect variation between the triplicate experiments, rather than analytical errors. As Student (1908) noted: "Any experiment may be regarded as forming an individual of a population of experiments which might be performed under the same conditions". The triplicates form a sample drawn from this population. To account for the uncertainty in the standard deviation of the population, a t distribution needs to be used, with significantly fatter tails than a normal distribution if the number of samples is less than 10. Since the number of samples ($n$) is equal to 3, we assume that the data are t-distributed with $n - 1 = 2$ degrees of freedom.

## Appendix B. Supplementary data

Supplementary material related to this article can be found online at https://doi.org/10.1016/j.jtbi.2024.111883.

## References

Bar-Even, A., Noor, E., Savir, Y., Liebermeister, W., Davidi, D., Tawfik, D.S., Milo, R., 2011. The moderately efficient enzyme: Evolutionary and physicochemical trends shaping enzyme parameters. Biochemistry 50, 4402–4410.

Berman, T., Chava, S., Kaplan, B., Wynne, D., 1991. Dissolved organic substrates as phosphorus and nitrogen sources for axenic batch cultures of freshwater green algae. Phycologia 30, 339–345.

Bolton, J.R., Hall, D.O., 1991. The maximum efficiency of photosynthesis. Photochem. Photobiol. 53, 545–548.

Bougaran, G., Bernard, O., Sciandra, A., 2010. Modeling continuous cultures of microalgae colimited by nitrogen and phosphorus. J. Theoret. Biol. 265, 443–454.

Boyer, K.E., Fong, P., Armitage, A.R., Cohen, R.A., 2004. Elevated nutrient content of tropical macroalgae increases rates of herbivory in coral, seagrass, and mangrove habitats. Coral Reefs 23, 530–538.

Bremer, H., Dennis, P.P., 1996. Modulation of chemical composition and other parameters of the cell by growth rate. In: Neidhardt, F.C. (Ed.), *Escherichia coli* and *Salmonella*: Cellular and Molecular Biology. American Society for Microbiology.

Broecker, W.S., 1982. Ocean chemistry during glacial time. Geochim. Cosmochim. Acta 46, 1689–1705.

Caperon, J., 1968. Population growth response of *Isochrysis galbana* to nitrate variation at limiting concentrations. Ecology 49, 866–872, URL: http://www.jstor.org/stable/1936538.

Caperon, J., Meyer, J., 1972. Nitrogen-limited growth of marine phytoplankton – Changes in population characteristics with steady-state growth rate. Deep-Sea Res. 19, 601–618.

Chien, C.T., Pahlow, M., Li, N., Oschlies, A., 2023. Effects of phytoplankton physiology on global ocean biogeochemistry and climate. Sci. Adv. 9, eadg1725.

Chiovitti, A., Molino, P., Crawford, S.A., Teng, R., Spurck, T., Wetherbee, R., 2004. The glucans extracted with warm water from diatoms are mainly derived from intracellular chrysolaminaran and not extracellular polysaccharides. Eur. J. Phycol. 39, 117–128.

Conover, S.A.M., 1975. Partitioning of nitrogen and carbon in cultures of the marine diatom *Thalassiosira fluviatilis* supplied with nitrate, ammonium, or urea. Mar. Biol. 32, 231–246.

Daines, S., Clark, J., Lenton, T., 2014. Multiple environmental controls on phytoplankton growth strategies determine adaptive responses of the N : P ratio. Ecol. Lett. 17, 414–425. http://dx.doi.org/10.1111/ele.12239, URL: http://www.ncbi.nlm.nih.gov/pubmed/24418348.

Deschamps, P., Haferkamp, I., d'Hulst, C., Neuhaus, H.E., Ball, S.G., 2008. The relocation of starch metabolism in chloroplasts: When, Why, and How. Trends Plant Sci. 13, 574–582.

Díaz, J., Ingall, E., Paterson, D., de Jonge, M.D., McNulty, I., Brandes, J.A., 2008. Marine polyphosphate: A key player in geologic phosphorus sequestration. Science 320, 652–655.

Droop, M.R., 1968. Vitamin $B_{12}$ and marine ecology. IV The kinetics of uptake, growth and inhibition in *Monochrysis lutheri*. J. Mar. Biol. Assoc. UK 48, 689–733, URL: http://journals.cambridge.org/abstract_S0025315400019238.

Droop, M.R., 1974. The nutrient status of algal cells in continuous culture. J. Mar. Biol. Assoc. UK 54, 825–855.

Dyhrman, S.T., 2016. Nutrients and their acquisition: Phosphorus physiology in microalgae. In: Borowitzka, M.A., Beardall, M.A., Raven, J.A. (Eds.), The Physiology of Microalgae. Springer International, Switzerland, pp. 155–183.

Edwards, K.F., Thomas, M.K., Klausmeier, C.A., Litchman, E., 2012. Allometric scaling and taxonomic variation in nutrient utilization traits and maximum growth rate of phytoplankton. Limnol. Oceanogr. 57, 554–566.

Elrifi, I.R., Turpin, D.H., 1985. Steady-state luxury consumption and the concept of optimum nutient ratios: A study with phosphate and nitrate limited *Selenastrum minutum* (Chlorophyta). J. Phycol. 21, 592–602.

Enjalbert, B., Cocaign-Bousquet, M., Portais, J.C., Letisse, F., 2015. Acetate exposure determines the diauxic behavior of *Escherichia coli* during the glucose-acetate transition. J. Bacteriol. 197, 3173–3181.

Enjalbert, B., Letisse, F., Portais, J.C., 2013. Physiological and molecular timing of the glucose to acetate transition in *Escherichia coli*. Metabolites 3, 820–837.

Falkowski, P.G., Raven, J.A., 2007. Aquatic Photosynthesis, second ed. Blackwell Science, Malden.

Finkel, Z.V., Follows, M.J., Liefer, J.D., Brown, C.M., Benner, I., Irwin, A.J., 2016. Phylogenetic diversity in the macromolecular composition of microalgae. PLoS One 11 (5), e0155977.

Flynn, K.J., 2001. A mechanistic model for describing dynamic multi-nutrient, light, temperature interactions in phytoplankton. J. Plankton Res. 23, 977–997.

Geider, R.J., Osborne, B.A., 1989. Respiration and microalgal growth: A review of the quantitative relationship between dark respiration and growth. New Phytol. 112, 327–341.

Geider, R.J., la Roche, J., 2002. Redfield revisited: Variability of C:N:P in marine microalgae and its biochemical basis. Eur. J. Phycol. 37, 1–17.

Ghyoot, C., Flynn, K.J., Mitra, A., Lancelot, C., Gypens, N., 2017. Modeling plankton mixotrophy: A mechanistic model consistent with the shuter-type biochemical approach. Front. Ecol. Evol. 5 (78).

Goldman, J.C., 1986. On phytoplankton growth rates and particulate C:N:P ratios at low light. Limnol. Oceanogr. 31, 1358–1363.

Halsey, K.H., Jones, B.M., 2015. Phytoplankton strategies for photosynthetic energy allocation. Annu. Rev. Mar. Sci. 7, 265–297.

Hastings, W.K., 1970. Monte Carlo sampling methods using Markov chains and their applications. Biometrika 57, 97–109.

Hessen, D.O., Elser, J.J., Sterner, R.W., Urabe, J., 2013. Ecological stoichiometry: An elementary approach using basic principles. Limnol. Oceanogr. 58, 2219–2236.

Hockin, N.L., Mock, T., Mulholland, F., Kopriva, S., Malin, G., 2012. The response of diatom central carbon metabolism to nitrogen starvation is different from that of green algae and higher plants. Plant Physiol. 158, 299–312.

Inomura, K., Omta, A.W., Talmy, D., Bragg, J., Deutsch, C., Follows, M.J., 2020. A mechanistic model of macromolecular allocation, elemental stoichiometry, and growth rate in phytoplankton. Front. Microbiol. 11, 86.

Jensen, E.L., Yangüez, K., Carrière, F., Gontero, B., 2020. Storage compound accumulation in diatoms as response to elevated $CO_2$ concentration. Biology 9 (5).

Klausmeier, C.A., Litchman, E., Daufresne, T., Levin, S.A., 2004. Optimal nitrogen-to-phosphorus stoichiometry of phytoplankton. Nature 429, 171–174.

Kooijman, S.A.L.M., 2000. Dynamic Energy and Mass Budgets in Biological Systems, second ed. Cambridge University Press, Cambridge, UK.

Lambert, B., 2018. A Student's Guide To Bayesian Statistics. SAGE, Thousand Oaks, CA.

Legovic, T., Cruzado, A., 1997. A model of phytoplankton growth on multiple nutrients based on the Michaelis–Menten-Monod uptake, Droop's growth and Liebig's law. Ecol. Model. 99, 19–31.

Li, H.M., Zhang, Y.Y., Han, X.R., Shi, X.Y., Rivkin, R.B., Legendre, L., 2016. Growth responses of *Ulva prolifera* to inorganic and organic nutrients: Implications for macroalgal blooms in the southern Yellow Sea, China. Sci. Rep. 6, 26498.

Liefer, J.D., Garg, A., Campbell, D.A., Irwin, A.J., Finkel, Z.V., 2018. Nitrogen starvation induces distinct photosynthetic responses and recovery dynamics in diatoms and prasinophytes. PLoS One 13, e0195705.

Liefer, J.D., Garg, A., Fyfe, M.H., Irwin, A.J., Benner, I., Brown, C.M., Follows, M.J., Omta, A.W., Finkel, Z.V., 2019. The macromolecular basis of phytoplankton C:N:P under starvation. Front. Microbiol. 10 (763).

Litchman, E., Klausmeier, C.A., Schofield, O.M., Falkowski, P.G., 2007. The role of functional traits and trade-offs in structuring phytoplankton communities: Scaling from cellular to ecosystem level. Ecol. Lett. 10, 1170–1181.

Lomas, M.W., Glibert, P.M., 2000. Comparisons of nitrate uptake, storage, and reduction in marine diatoms and flagellates. J. Phycol. 36, 903–913.

Metropolis, N., Rosenbluth, A.W., Rosenbluth, M.N., Teller, A.H., Teller, E., 1953. Equations of state calculations by fast computing machines. J. Chem. Phys. 21, 1087–1092.

Moreno, A.R., Martiny, A.C., 2018. Ecological stoichiometry of ocean plankton. Annu. Rev. Mar. Sci. 10, 43–69.

Nicholson, D.P., Stanley, R.H.R., Doney, S.C., 2018. A phytoplankton model for the allocation of gross photosynthetic energy including the trace-offs of diazotrophy. J. Geophys. Res.: Biogeosci. 123, 1796–1816.

Omta, A.W., Bruggeman, J., Kooijman, S.A.L.M., Dijkstra, H.A., 2006. The biological carbon pump revisited: Feedback mechanisms between climate and the redfield ratio. Geophys. Res. Lett. 33 (L14613), http://dx.doi.org/10.1029/2006GL026213.

Omta, A.W., Bruggeman, J., Kooijman, S.A.L.M., Dijkstra, H.A., 2009. The organic carbon pump in the Atlantic. J. Sea Res. 62, 179–187.

Omta, A.W., Kooijman, S.A.L.M., Dijkstra, H.A., 2007. The influence of (sub-)mesoscale eddies on the soft-tissue carbon pump. J. Geophys. Res. - Oceans (112), http://dx.doi.org/10.1029/2007JC004189.

Omta, A.W., Talmy, D., Inomura, K., Irwin, A.D., Finkel, Z.V., Sher, D., Liefer, J.D., Follows, M.J., 2020. Quantifying nutrient throughput and DOM production by algae in continuous culture. J. Theoret. Biol. 494, 110214.

Omta, A.W., Talmy, D., Sher, D., Finkel, Z.V., Irwin, A.D., Follows, M.J., 2017. Extracting phytoplankton physiological traits from batch and chemostat culture data. Limnol. Oceanogr.: Methods 15, 453–466.

Pahlow, M., 2005. Linking chlorophyll-nutrient dynamics to the redfield N:C ratio with a model of optimal phytoplankton growth. Mar. Ecol. Prog. Ser. 287, 33–43.

Pahlow, M., Oschlies, A., 2013. Optimal allocation backs Droop's cell-quota model. Mar. Ecol. Prog. Ser. 473, 1–5.

Palenik, B., Morel, F.M.M., 1991. Amine oxidases of marine phytoplankton. Appl. Environ. Microbiol. 57, 2440–2443.

Pantoja, S., Lee, C., 1994. Cell–surface oxidation of amino acids in seawater. Limnol. Oceanogr. 39, 1718–1726.

Parslow, J.S., Harrison, P.J., Thompson, P.A., 1984. Saturated uptake kinetics: Transient response of the marine diatom *Thalassiosira pseudonana* to ammonium, nitrate, silicate or phosphate starvation. Mar. Biol. 83, 51–59.

Plath, K., Boersma, M., 2001. Mineral limitation of zooplankton: Stoichiometric constraints and optimal foraging. Ecology 82, 1260–1269.

Quigg, A., Finkel, Z.V., Irwin, A.J., Rosenthal, Y., Ho, T.Y., Reinfelder, J.R., Schofield, O., Morel, F.M.M., Falkowski, P.G., 2003. The evolutionary inheritance of elemental stoichiometry in marine phytoplankton. Nature 425, 291–294.

Ral, J.P., Derelle, E., Farraz, C., Wattebled, F., Farinas, B., Corellou, F., Buléon, A., Slomianny, M.C., Delvalle, D., d'Hulst, C., Rombbauts, S., Moreau, H., Ball, S., 2004. Starch division and partitioning. A mechanism for granule propagation and maintenance in the picophytoplanktonic green alga *Ostreococcus tauri*. Plant Physiol. 136, 3333–3340.

Raven, J.A., 1987. The role of vacuoles. New Phytol. 106, 357–422.

Rhee, G.Y., 1973. A continuous culture study of phosphate uptake, growth rate and polyphosphate in *Scenedesmus* sp. J. Phycol. 9, 495–506, URL: http://onlinelibrary.wiley.com/doi/10.1111/j.1529-8817.1973.tb04126.x/abstract.

Rhee, G.Y., 1978. Effects of N:P limitation on algal growth, cell composition, and nitrate uptake. Limnol. Oceanogr. 23, 10–24.

Riper, D.M., Owens, T.G., Falkowski, P.G., 1979. Chlorophyll turnover in *Skeletonema costatum*, a marine plankton diatom. Plant Physiol. 64, 49–54.

Rothhaupt, K.O., 1995. Algal nutrient limitation affects rotifer growth rate but not ingestion rate. Limnol. Oceanogr. 40, 1201–1208.

Scott, M., Gunderson, C.W., Matescu, E.M., Zhang, Z., Hwa, T., 2010. Interdependence of cell growth and gene expression: Origins and consequences. Science 330, 1099–1102.

Sharoni, S., Halevy, I., 2020. Nutrient ratios in marine particulate organic matter are predicted by the population structure of well-adapted phytoplankton. Sci. Adv. 6, eaaw9731.

Shuter, B., 1979. A model of physiological adaptation in unicellular algae. J. Theor. Biol 78, 519–552, URL: http://www.ncbi.nlm.nih.gov/pubmed/513795.

Sicko-Goad, L.M., Schelske, C.L., Stoermer, E.F., 1984. Estimation of intracellular carbon and silica content of diatoms from natural assemblages using morphometric techniques. Limnol. Oceanogr. 29, 1170–1178.

Simionato, D., Block, M.A., Rocca, N.la., Jouhet, J., Maréchal, E., Finazzi, G., Morosinotto, T., 2013. The response of *Nannochloropsis gaditana* to nitrogen starvation includes *De Novo* biosynthesis of triacylglycerols, a decrease of chloroplast galactolipids, and reorganization of the photosynthetic apparatus. Eukaryot. Cell 12, 665–676.

Sipler, R.E., Bronk, D.A., 2015. Dynamics of Dissolved Organic Nitrogen. In: Hansell D.A. Carlson, C.A (Eds.), Biogeochemistry of Marine Dissolved Organic Matter, second ed. Elsevier Inc., The Netherlands, pp. 127–232.

Smith, S.L., Merico, A., Hohn, S., Brandt, G., 2014. Sizing-up nutrient uptake kinetics: Combining a physiological trade-off with size-scaling of phytoplankton traits. Mar. Ecol. Prog. Ser. 511, 33–39.

Solovchenko, A.E., Ismagulova, T.T., Lukyanov, A.A., Vasilieva, S.G., Konyukhov, I.V., Pogosian, S.I., Lobakova, E.S., Goreleva, O.A., 2019. Luxury phosphorus uptake in microalgae. J. Appl. Phycol. 31, 2755–2770.

Sonoike, K., 2011. Photoinhibition of photosystem I. Physiol. Plant. 42, 56–64.

Sterner, R.W., Elser, J.J., 2002. Ecological Stoichiometry. Princeton University Press, Princeton.

Sterner, R.W., Hessen, D.O., 1994. Algal nutrient limitation and the nutrition of aquatic herbivores. Annu. Rev. Ecol. Syst. 25, 1–29.

Student, 1908. The probable error of the mean. Biometrika 6, 1–25.

Sukenik, A., Kaplan-Levy, R.N., Welch, J.M., Post, A.F., 2012. Massive multiplication of genome and ribosomes in dormant cells (akinetes) of *Aphanizomenon ovalisporum* (*cyanobacteria*). ISME J. 6, 670–679.

Sundya, S., Delvigne, F., Uribelarrea, J.L., Molina-Jouve, C., Gorret, N., 2012. Comparison of the transient responses of *Escherichia coli* to a glucose pulse of various intensities. Appl. Microbiol. Biotechnol. 95, 1021–1034.

Talmy, D., Blackford, J., Hardman-Mountford, N., Polimene, L., Follows, M., Geider, R., 2014. Flexible C:N ratio enhances metabolism of large phytoplankton when resource supply is intermittent. Biogeosciences 11, 4881–4895. http://dx.doi.org/10.5194/bgd-11-5179-2014, URL: http://www.biogeosciences-discuss.net/11/5179/2014/.

Taylor, K.E., 2001. Summarizing multiple aspects of model performance in a single diagram. J. Geophys. Res. - Atmos. 106, 7183–7192.

Terry, K.L., 1982. Nitrate uptake and assimilation in *Thalassiosira weissflogii* and *Phaeodactylum tricornutum*: Interactions with photosynthesis and with the uptake of other ions. Mar. Biol. 69, 21–30.

Thangaraj, S., Palanisamy, S.K., Zhang, G., Sun, J., 2021. Quantitative proteomic profiling of marine diatom *Skeletonema dohrnii* in response to temperature and silicate induced environmental stress. Front. Microbiol. 11, 554832.

Tolonen, A.C., Aach, J., Lindell, D., Johnson, Z.I., Rector, T., Steen, R., Church, G.M., Chisholm, S.W., 2006. Global gene expression of *Prochlorococcus* ecotypes in response to changes in nitrogen availability. Mol. Syst. Biol. 3 (53).

Toseland, A., Daines, S.J., Clark, J.R., Kirkham, A., Strauss, J., Uhlig, C., Lenton, T.M., Valentin, K., Pearson, G.A., Moulton, V., Mock, T., 2013. The impact of temperature on marine phytoplankton resource allocation and metabolism. Nature Clim. Change 3, 979–984.

Vass, I., 2012. Molecular mechanisms of photodamage in the Photosystem II complex. Biochim. Biophys. Acta Bioenerg. 1817, 209–217.

Volk, T., Hoffert, M.I., 1985. Ocean carbon pumps: Analysis of relative strengths and efficiencies in ocean-driven atmospheric $CO_2$. In: Sundquist, E.T., Broecker, W.S. (Eds.), The Carbon Cycle and Atmospheric $CO_2$: Natural Variations Archean To Present. AGU, Washington D.C., pp. 99–110.

Ward, B.A., Follows, M.J., 2016. Marine mixotrophy increases trophic transfer efficiency, mean organism size, and vertical carbon flux. Proc. Natl. Acad. Sci. 113, 2958–2963.

Wirtz, K.W., Pahlow, M., 2010. Dynamic chlorophyll and nitrogen:carbon regulation in algae optimizes instantaneous growth rate. Mar. Ecol. Prog. Ser. 402, 81–96.

Wu, C., Xiong, W., Dai, J., Wu, Q., 2015. Genome-based metabolic mapping and $^{13}C$ flux analysis reveal systematic properties of an oleaginous microalga *Chlorella protothecoides*. Plant Physiol. 167, 586–599.

Zavafer, A., 2021. A theoretical framework of the hybrid mechanism of Photosystem II photodamage. Photosynth. Res. 149, 107–120.

Zimmerman, A.E., Podowski, J.C., Gallagher, G.E., Coleman, M.L., Waldbauer, J.R., 2023. Tracking nitrogen allocation to proteome biosynthesis in a marine microbial community. Nat. Micorbiol. 8, 498–509.